ARMA 24–0019

Strength Characteristics of Highly Anisotropic Burst-Prone Coal Considering Mineralogical Compositions

Kim, B.H. and M.K. Larson

CDC/NIOSH, Spokane, Washington, United States

ABSTRACT: This paper was developed as part of an effort by the National Institute for Occupational Safety and Health (NIOSH) to identify risk factors associated with bursts/bumps in the prevention of fatalities and accidents in highly stressed, burst- or bump-prone ground conditions. In this study, we evaluated the effects of different shapes and distribution densities of mineral grains in coal on failure mechanics using the numerical software 3DEC. The main aim of this study was to identify possible failure mechanisms influenced by mineral habit and frequency in coal. Exploring differences in failure mechanics associated with the mineral grains helped to determine the role of mineral character as a possible contributor to characterize burst-prone coals. To achieve the goal of this study, a series of numerical specimens were prepared in the 3DEC model as follows: first, the 3DEC modeling in conjunction with the DFNs (Discrete Fracture Networks) technique was performed to explicitly generate the discontinuities (i.e., cleats and bedding planes) in the numerical specimens based on the results of laboratory analyses. Then, the different realizations of mineral grains were embedded in the 3DEC model to simulate an unconfined compressive strength (UCS) test to assess the influence of the mineralogical characteristics on the UCS.

1. INTRODUCTION

The type of catastrophic failure in coal mines known as dynamic failure—also colloquially referred to as bumps, bounces, bursts, and others—is one of the most challenging and persistent engineering problems associated with coal mining in highly stressed conditions. Coal pillar bursts involve the sudden expulsion of coal and rock into the mine opening. These events occur when stresses in a coal pillar, left for support in underground workings, exceed the pillar's critical capacity, causing the pillar to rupture without warning. These events can be exceptionally violent, ejecting coal and rock with explosive force (Peng 2008; Kim and Larson 2017). Many uncertainties remain in the highly anisotropic characteristics of coal seams associated with geologic structure and spatial redistribution of induced stress in coal pillars due to mining activities (Kim et al. 2018; Kim and Larson 2021). Thus, to prevent fatalities, continuous effort is required to better understand this type of catastrophic failure mechanism in coal mines. This paper is developed as part of an effort by the National Institute for Occupational Safety and Health (NIOSH) to identify risk factors associated with bumps to prevent fatalities and accidents in highly stressed, bump-prone ground conditions.

Lawson (2020) explored how the geochemical and petrographic components of coal may impact its physical properties and how these components correlate with a history of reportable dynamic failure in coal mines. The results indicated that bumping coals from the United States are generally less mature, lower in carbon, lower in sulfur and particularly lower in pyritic sulfur, lower in mineral matter, higher in oxygen, softer, and less well cleated than coals that do not bump. Of these correlations, the correlation between dynamic failure occurrence and low pyritic sulfur content was by far the strongest. However, it is unclear whether the correlation between pyritic sulfur content, gross mineral matter content, and a history of dynamic failure accidents exists as a proxy for risk associated with geologic setting, whether it impacts the properties of the coal itself, or whether it is entirely unrelated. Ye et al. (2013) investigated the influence of horizontal restraint, existence, and different geometric distribution of pyrite particles on mechanical behavior and the failure process of high-sulfur coal as applied to crushing operations. They concluded that the compressive strength of coal containing a pyrite particle was greater than that of pure coal, and that there was higher stress concentration when the pyrite particle was located in the upper and lower parts of the coal sample, thus contributing to the failure process. When the pyrite particle was located in the center of the coal sample, the compressive strength was higher than that of the other positions in the sample.

In this study, we evaluated the effects of different shapes and distribution densities of stiff mineral grains in the coal on failure mechanics using 3DEC (Itasca Consulting Group 2019). Mineral grain frequencies are based on a sampling of low- and high-sulfur coals from the

Pennsylvania State Coal Sample Databank. The purpose of this study is to identify possible failure mechanisms associated with mineral habit and frequency in coal. Exploring differences in failure mechanics associated with pyrite and other mineral grains will help to determine the role of mineral character as a possible contributor to the correlation between dynamic-failure-prone coals and low pyritic sulfur and mineral content.

The next section introduces the stochastic simulation approach used for mineral grain geometry generation using MATLAB. The next section describes the approach for the numerical modeling, including assumptions and conditions. Finally, methodologies appropriate to evaluate the effects of different shapes and distribution densities of mineral grains as the stiff grains in the coal are explained and demonstrated by means of the DFNs (Discrete Fracture Networks) and 3DEC modeling.

2. PYRITE GEOMETRY GENERATION USING MATLAB AND ITS IMPLEMENTATION IN 3DEC

As low pyritic sulfur content and mineral matter in general have been associated with reportable dynamic failures in the United States on an empirical basis, we explored two common shapes of mineral grains, rectangular and framboidal, as illustrated in Fig. 1. The latter is common to pyrite forming in coal and often appears in clusters. The framboidal shapes are nearly round, but with some slightly undulating surfaces. The rectangular shape may be more representative of carbonates and silicates, although this is of necessity a gross simplification of the irregularity that occurs in nature. Further, it is important to note that not all minerals or mineral habits that may occur in coal are represented in this study, but rather this is a general exploration of how some common mineral habits at different compositional frequencies may impact mechanical behavior of coal under load.

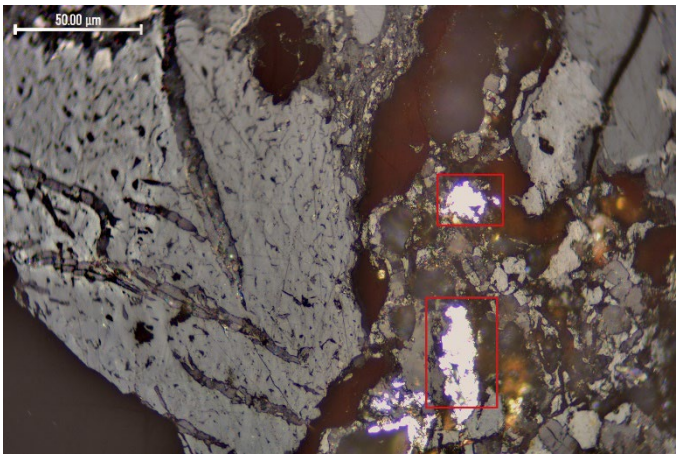

Fig. 1. Example of framboidal pyrite geometry (in red square and rectangle).

A series of mineral grain geometries were generated using MATLAB for random nonoverlapping placement of grains. Three specific realizations for each of the model sets were used as the baseline geometry sources for the 3DEC model that were rectangular minerals (2% of volume), rectangular minerals (9%), and clustered framboidal pyrite (2%). The MATLAB outputs provided digital representation of these shapes in two-dimensions, dispersed in a representative way, with various orientations. The orientations chosen were those with the long axes pointed at 0°, 15°, 30°, 45°, 60°, and 90° with respect to horizontal in a specimen that was 5-cm wide and 10-cm high. Fig. 2 shows examples of the mineral grain geometries generated using MATLAB.

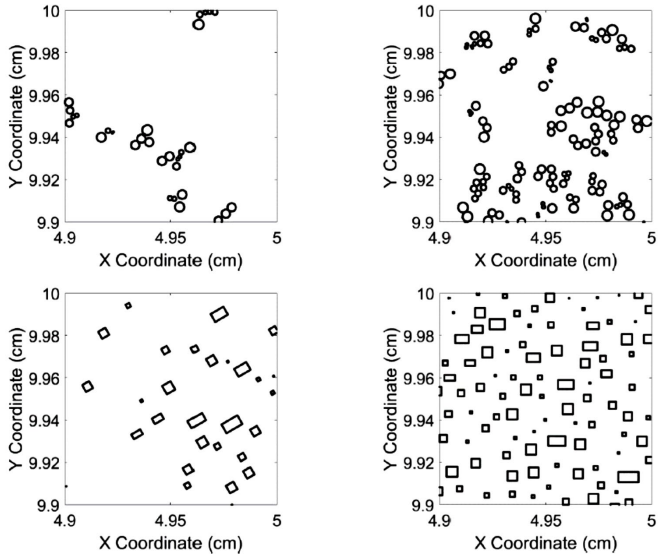

Fig. 2. Pyrite Realizations by MATLAB (top row: clustered framboidal pyrite; bottom row: rectangular pyrite; left column: 2.0% pyrite; right column: 9.0% pyrite).

The rectangular grains generated had 140 vertices for each grain in a clockwise direction. To simplify, a LabTalk script was used with OriginPro 2019b software (OriginLab Corporation 2021) to select only the corner vertices and output them to a file. A custom Fortran code was written that targeted the number of grains to be either an input number of grains or an input percentage of the two-dimensional specimen's area. The code then output a file having 3DEC block generation commands that constructed the grains as blocks formed by faces.

The framboidal grains digitized and then generated by MATLAB had 126 vertices for each grain in a counterclockwise direction. As seen in Fig. 3, the grain generated is not a completely convex polygon, as required by 3DEC. In addition, the grains were pseudo 2D, meaning that they had a small thickness. The number of faces required to generate just one grain made the problem size too large to be practical for a 3DEC model. To overcome both challenges, polygons were determined from the MATLAB-generated polygons by skipping 13 vertices—that is, selecting every 14th vertex. As seen in

Fig. 3, the polygon thus generated is simplified to a nonagon, yet it approximates the polygon formed by all the vertices and has no concave angles. As for the rectangular grains, a custom Fortran code was written to select the number of grains to be converted into 3DEC block generation commands by inputting either a few grains or a percentage of the two-dimensional specimen's area. The code then output a file having 3DEC block generation commands that constructed the grains as blocks formed by faces.

Since the MATLAB output files were very large for each of these cases, this automated approach was necessary to convert the mineral grain vertices into 3DEC blocks. By this approach, a total of 6 different cases for no mineral grains, cases of 0.5%, 2%, and 9% rectangular mineral grains, and cases of 0.5% and 2% clustered framboidal pyrite were prepared and then used to construct 3DEC models.

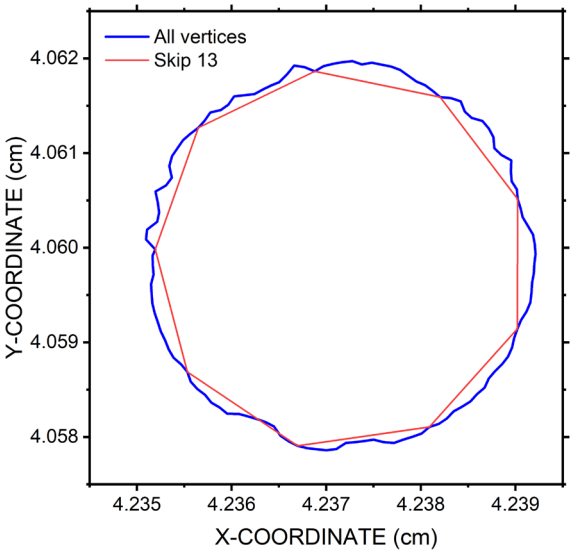

Fig. 3. Example of a framboidal grain with all 126 vertices and a grain approximating it formed by skipping 13 vertices (using only every 14th vertex).

The built-in DFN generator in 3DEC was used to explicitly realize the spatial anisotropic characteristics of the discontinuities (i.e., cleats and bedding planes) in the coal specimens. The different dip angles of the bedding planes were used to generate the DFNs that more explicitly represent two anisotropies of coal in a 0.5-cm (W) x 1-cm (H) x 0.05-cm (D) numerical domain. Two sets of bedding planes are presented in this section, having mean dip angles of 0° and 30° from horizontal. The realized mineral grains (50-μm diameter or edge lengths with 2-μm thickness) were imported into the 3DEC model and then were considered as a stiff mineral inclusion. The Young's modulus of the mineral grains selected was approximately 12 times greater than that of the intact coal matrix for both mineral habits.

Fig. 4 presents the 3DEC model that shows the intact coal matrix (grey), imported mineral grain geometry (yellow), and cleats and bedding planes (dark grey).

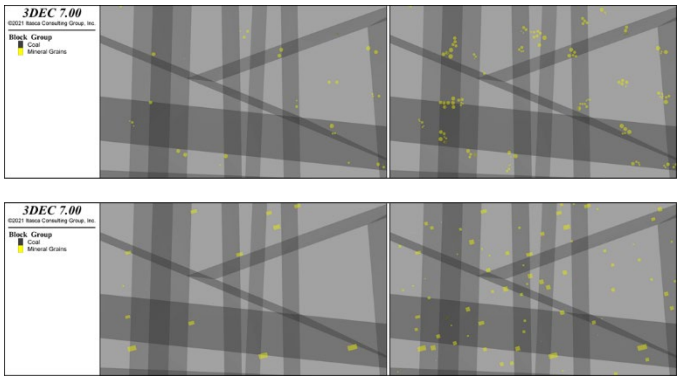

Fig. 4. The 3DEC models showing intact coal matrix mineral grains and discontinuities (top: 0.5% and 2% framboidal pyrite, bottom: 0.5% and 2% rectangular mineral grains).

All blocks in the 3DEC model were built as deformable elastic blocks. The heterogeneity of the engineering properties (i.e., cohesion and tensile strength) in the 3DEC models was also considered using Monte Carlo simulations. Heterogeneous strengths were modeled by populating the blocks and block contacts of the model using triangular probability distributions. The built-in Mohr C++ plug-in was used in the models. To create the numerical specimens, each block contact was assigned a cohesion and a tensile strength value randomly selected from the probability distributions generated by the Monte Carlo simulation. The baseline material properties were considered from the results of laboratory tests (Kim et al., 2018; Kim and Larson, 2021). The ranges of the cohesion and the tensile strength were 1.35±0.91 MPa and 0.45±0.30 MPa, respectively. All sub-contacts forming each contact were assigned the same tensile strength and cohesion.

Table 1 shows the input data used for the 3DEC model.

Table 1. Input data for the coal and pyrite in the 3DEC model

Zone Group	Young's Modulus (GPa)	Poisson's Ratio	Joint properties (cleats and bedding planes)					Remark
			Normal stiffness (GPa/m/m)	Shear stiffness (GPa/m/m)	Cohesion (MPa)	Friction Angle (°)	Tensile strength (MPa)	
Intact coal	9.0	0.25	105	52.5	1.35 (±0.91)	35	0.45 (±0.3)	Mohr model
Mineral grains	110.0	0.15	-	-	-	-	-	Elastic model

3. RESULTS AND DISCUSSION

Unconfined compressive strength (UCS) test simulations were carried out using the constructed 3DEC models. The results of the 3DEC modeling allowed for initial assessment of hypotheses related to the observation of low mineral matter and very low pyritic sulfur in coals prone to dynamic failure.

Fig. 5 presents the block displacements and the joint shear displacements in the synthetic well-cleated coal specimens with a 0°–90° included angle which is the angle between the discontinuities (cleats and bedding planes) and loading direction. Fig. 6 indicates the block displacements and the joint shear displacements in the synthetic, well-cleated coal specimens with a 30°–60° included angle.

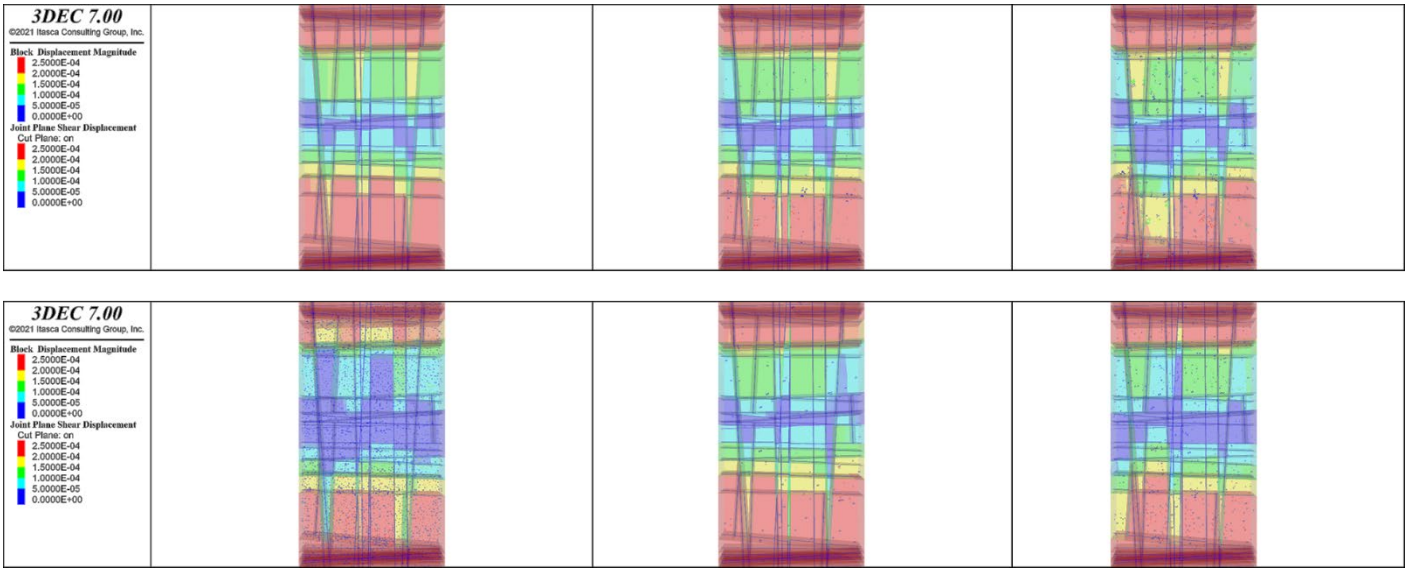

Fig. 5. Block displacements and the joint shear displacements with well-cleated in 0°–90° included angle (top left to right: no pyrite, 0.5%, and 2% rectangular mineral grains; bottom left to right: 9% rectangular, 0.5% framboidal, and 2% framboidal pyrite).

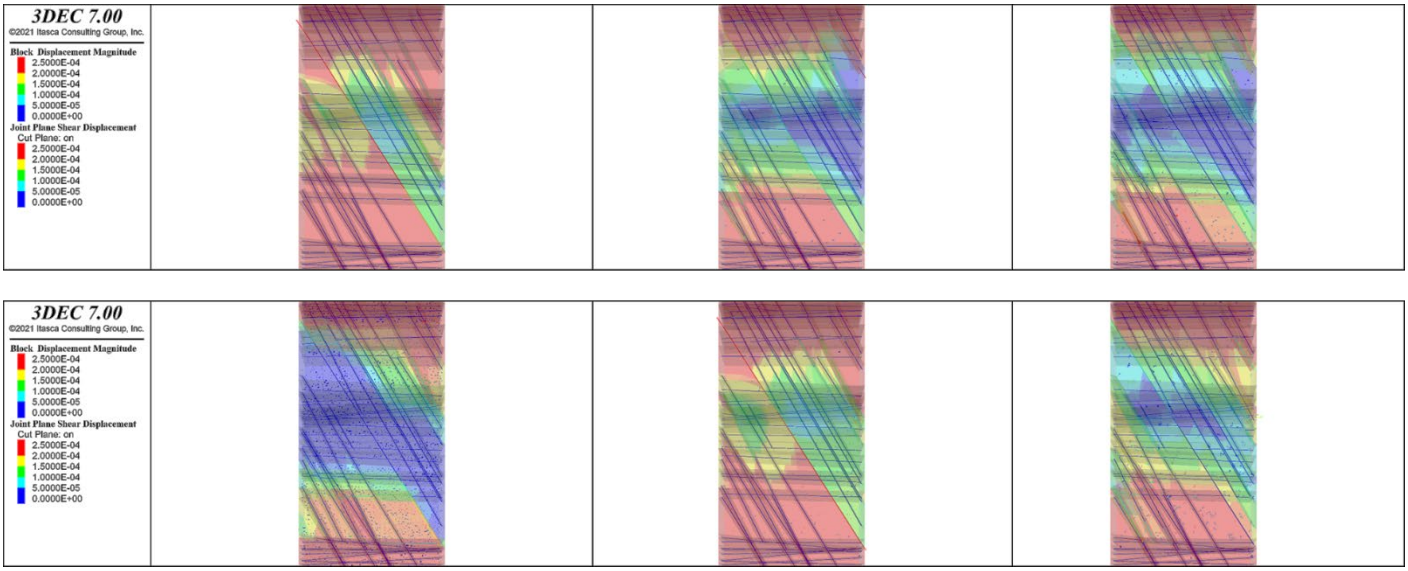

Fig. 6. Block displacements and the joint shear displacements with well-cleated in 30°–60° included angle (top left to right: no mineral grains, 0.5%, and 2% rectangular mineral grains; bottom left to right: 9% rectangular, 0.5% framboidal, and 2% framboidal pyrite).

Fig. 7 presents the block displacements and the joint shear displacements in the synthetic moderately-cleated coal specimens with a 0°–90° included angle. Fig. 8 indicates the block displacements and the joint shear displacements in the synthetic moderately cleated coal specimens with a 30°–60° included angle.

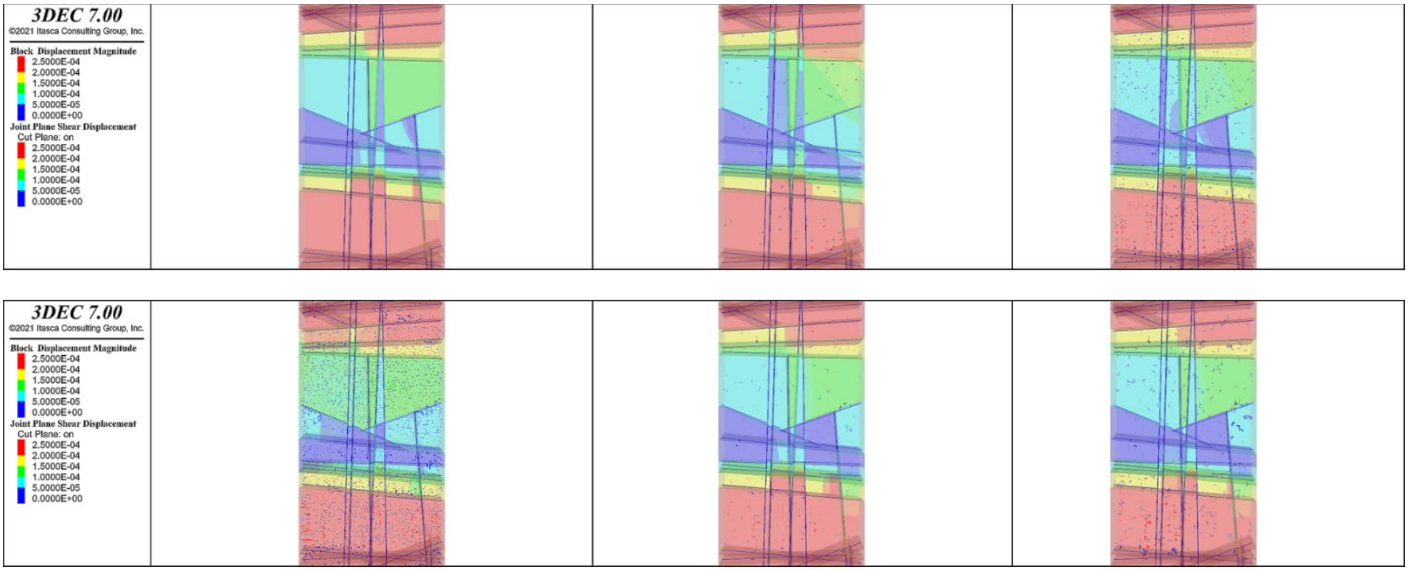

Fig. 7. Block displacements and the joint shear displacements with moderately cleated in 0°–90° included angle (top left to right: no mineral grains, 0.5%, and 2% rectangular mineral grains; bottom left to right: 9% rectangular, 0.5% framboidal, and 2% framboidal pyrite).

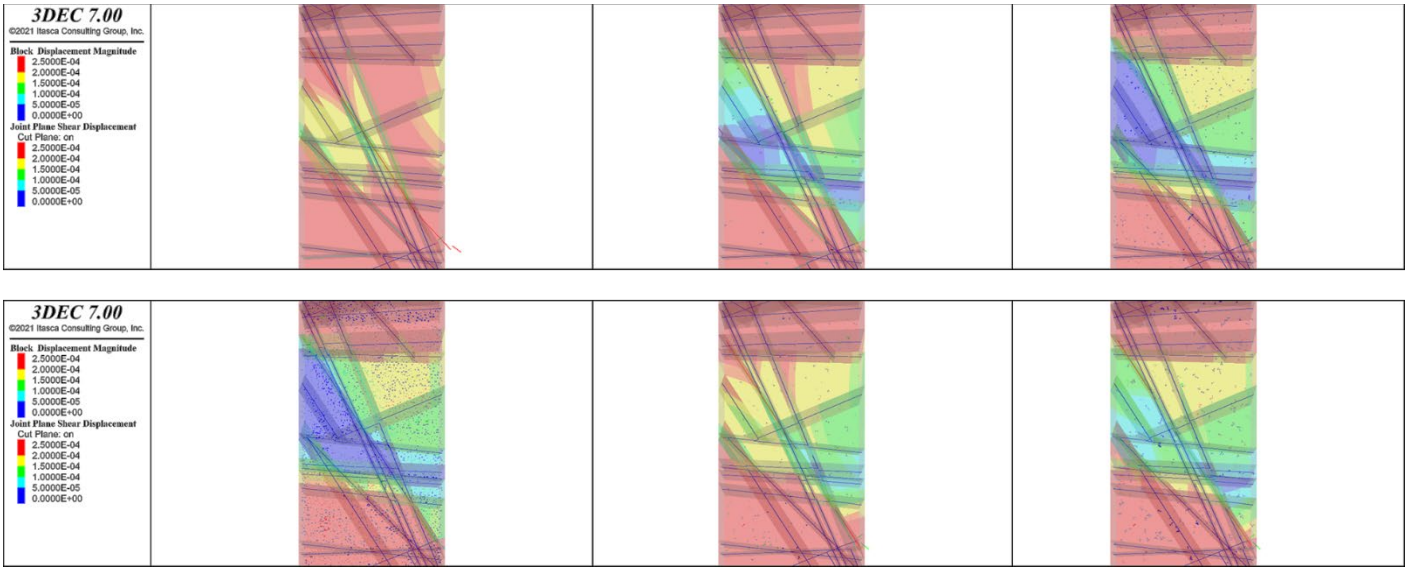

Fig. 8. Block displacements and the joint shear displacements with moderately cleated in 30°–60° included angle (top left to right: no mineral grains, 0.5%, and 2% rectangular mineral grains; bottom left to right: 9% rectangular, 0.5% framboidal, and 2% framboidal pyrite).

Fig. 9 presents the block displacements and the joint shear displacements in the synthetic poorly cleated coal specimens with a 0°–90° included angle. Fig. 10 indicates the block displacements and the joint shear displacements in the synthetic poorly cleated coal specimens with a 30°–60° included angle.

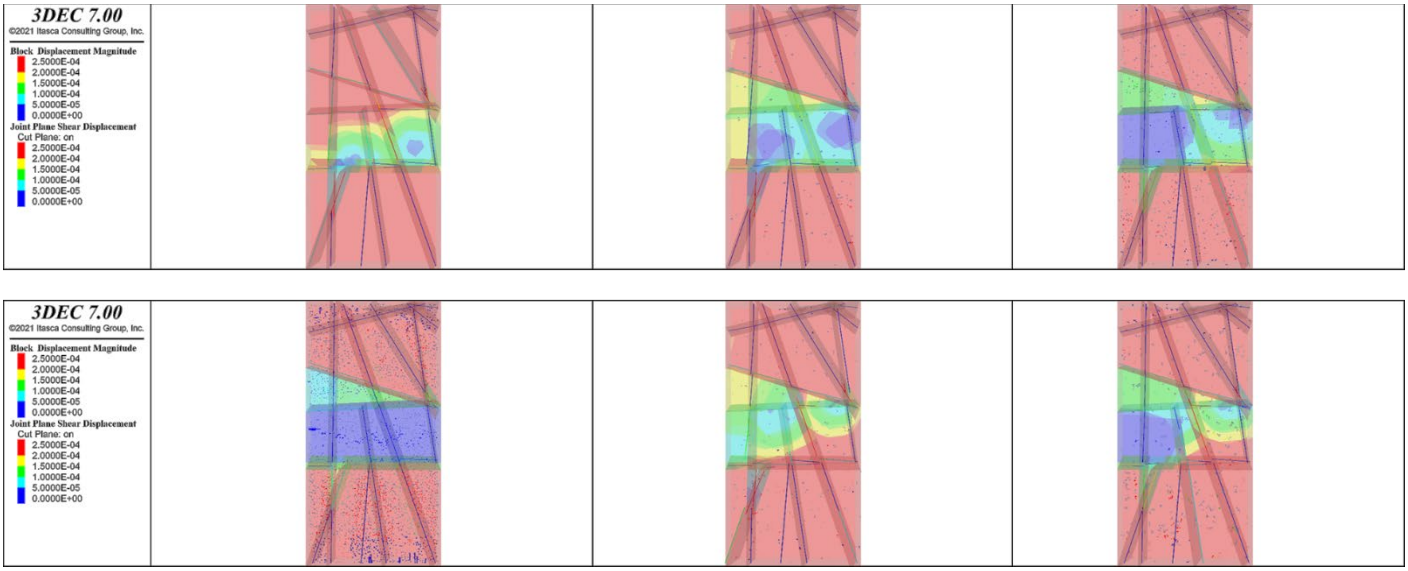

Fig. 9. Block displacements and the joint shear displacements with poorly cleated in 0°–90° included angle (top left to right: no mineral grains, 0.5%, and 2% rectangular mineral grains; bottom left to right: 9% rectangular, 0.5% framboidal, and 2% framboidal pyrite).

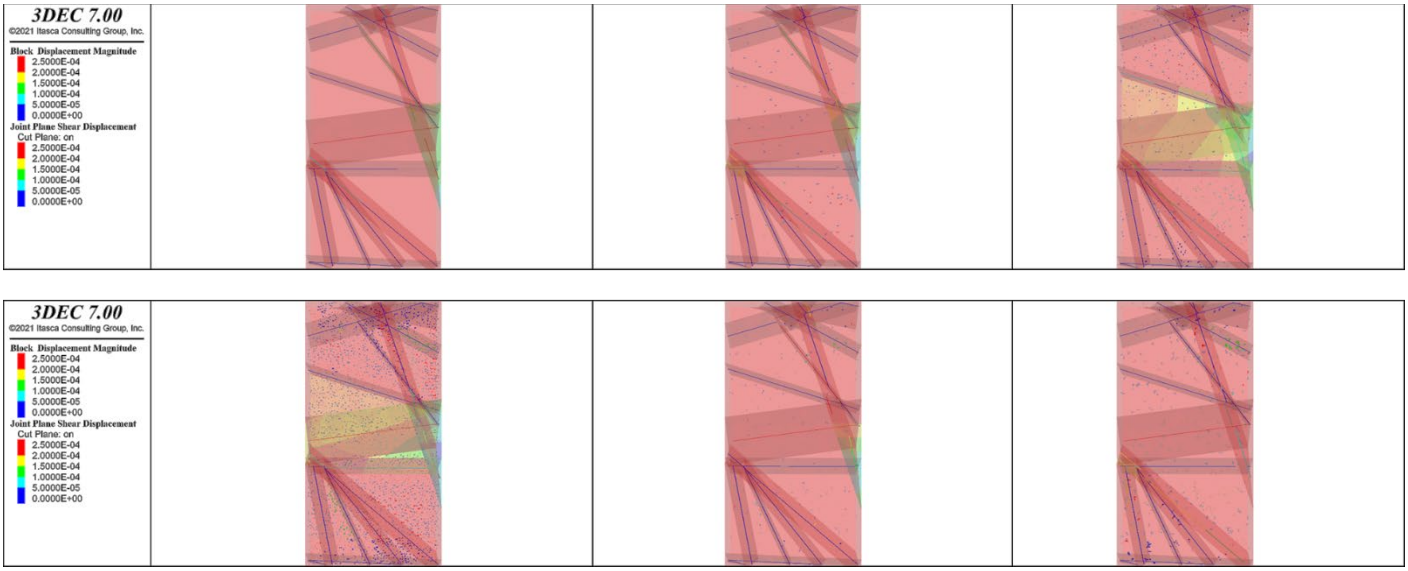

Fig. 10. Block displacements and the joint shear displacements with poorly cleated in 30°–60° included angle (top left to right: no pyrite, 0.5%, and 2% rectangular pyrite; bottom left to right: 9% rectangular, 0.5% framboidal, and 2% framboidal pyrite).

The major displacements in the cases having a 0°–90° included angle were caused by compression at both the top and the bottom of the intact coal matrix indicated as the dark red contours, whereas shear displacements along cleats were dominant in the cases of the 30°–60° included angle. These behaviors agreed well with the anisotropic characteristics documented in the literature (Kim et al., 2018, Kim and Larson, 2021). The different sizes of the blue contours in the figures allowed qualitative assessment of the influence of the mineral grain shape and volume proportion on the coal specimen behavior. The case of 9% rectangular mineral grains generally resulted in the relatively small block displacements illustrated as the extended blue contours.

Fig. 11 shows axial peak stress as a function of the mineral grain shapes and volume proportion with the various included angle and degree of cleats development. Because the 3DEC model dimensions were too small to perform a standard (i.e., ASTM or ISRM suggested) UCS test simulation, we determined a target axial strain as 0.005 and then measured an axial peak stress when the model reached the target axial strain. Fig. 11 (a) and (b) show the coal strength to be highly dependent on the degree of cleat development when the included angle is 0°–90°. However, when the included angle is 30°–60°, the coal strength becomes relatively independent of the degree of cleat development. In addition, the coal strength anisotropy is highly dependent on a poor degree of cleats development as shown in Fig. 11 (c).

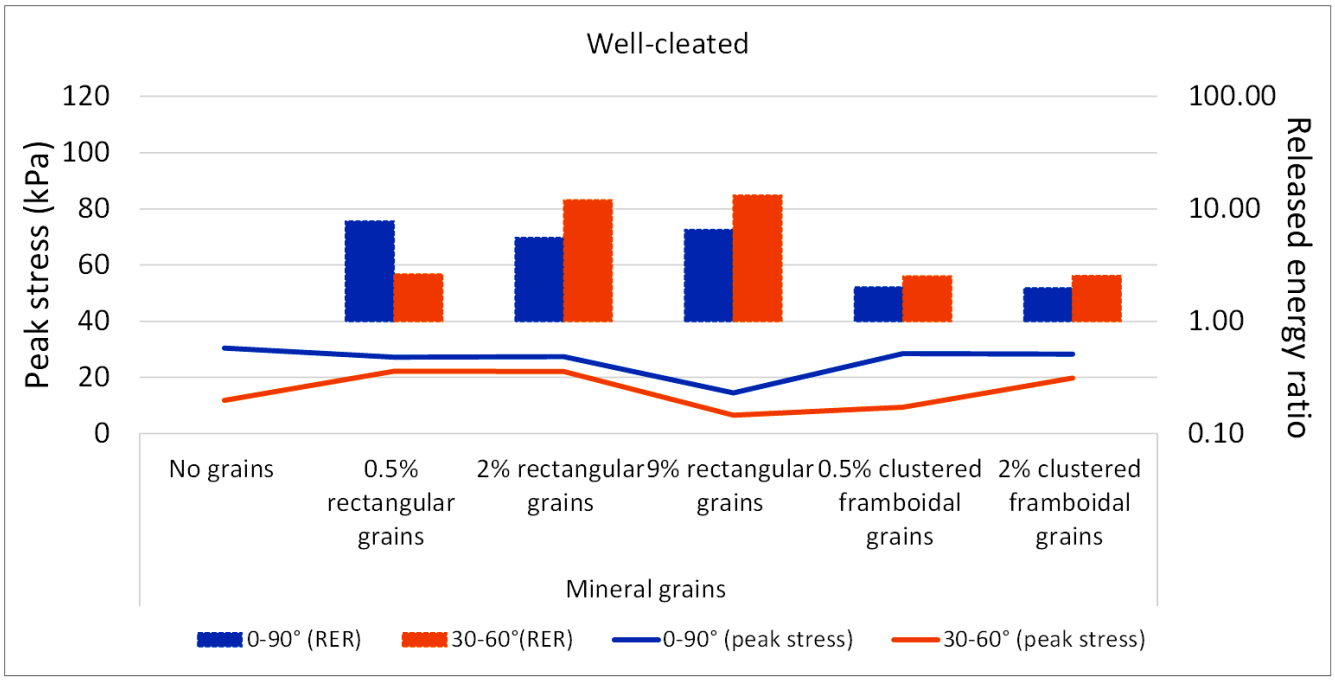

(a)

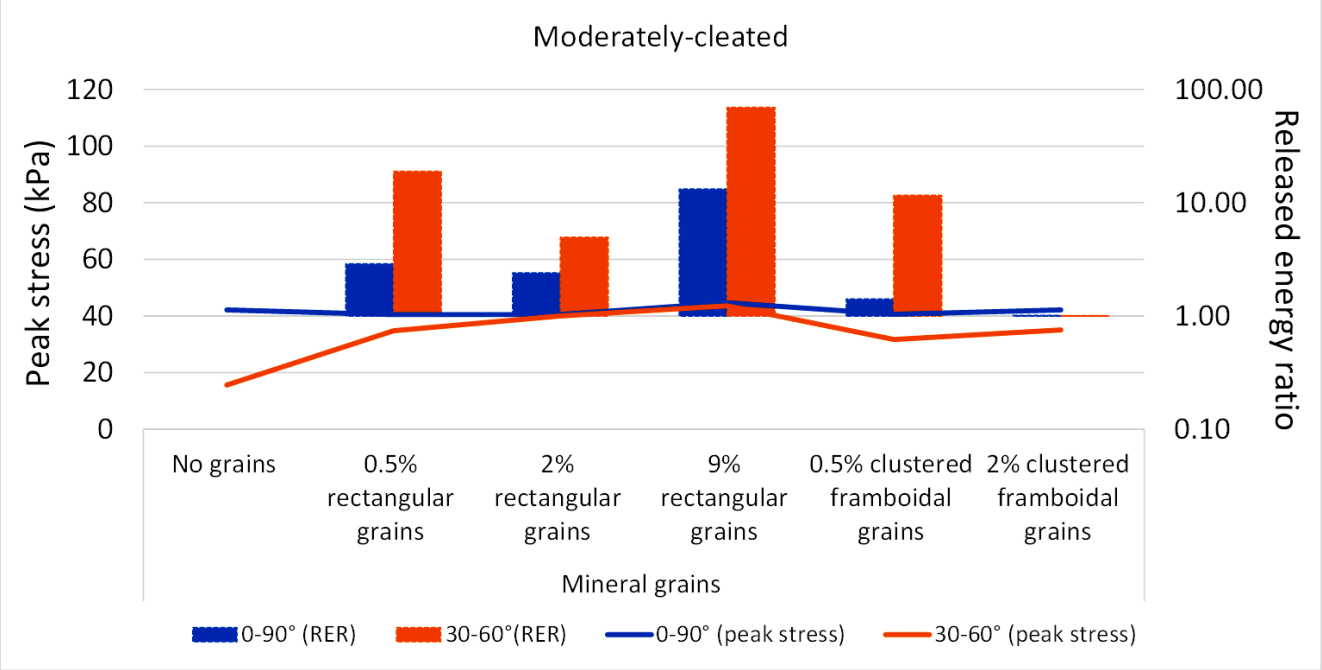

(b)

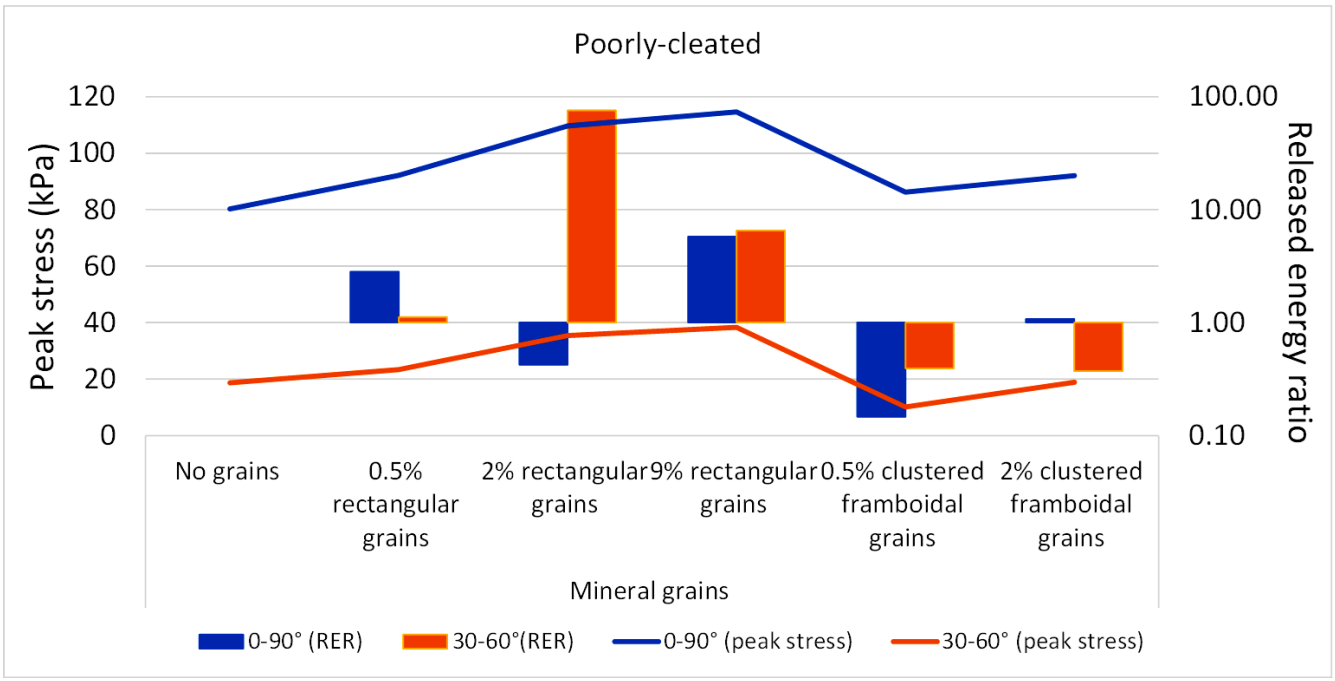

(c)

Fig. 11. Axial peak stress versus included angle/cleats developments/mineral grain volume — (a): well-cleated; (b) moderately-cleated; and (c) poorly-cleated.

Cai et al. (2015) reported that a difference in density between the matrix and mineral matter may weaken the cohesion of the coal, which could be a possible reason for the created fractures propagating along the junction of minerals and matrix.

Fig. 12 and Fig. 13 indicate the updated tensile strength in the mineral grain and discontinuity contacts for the case of 9% rectangular mineral grain with the various degrees of cleat development. The red contours illustrate a higher value of the tensile strength than the blue contours. As a result, as the cleats are moderately or poorly developed, the high volume of mineral content played a pivotal role in increasing the synthetic coal strength by working as an aggregate. The mineral grains possibly contributed as aggregates by providing an additional bonding strength to the synthetic moderately/poorly cleated coal. However, if the cleats were well developed, the high volume of mineral content contributed to a decrease in the synthetic

coal strength as a micro-defect in conjunction with the well-cleated system in coal.

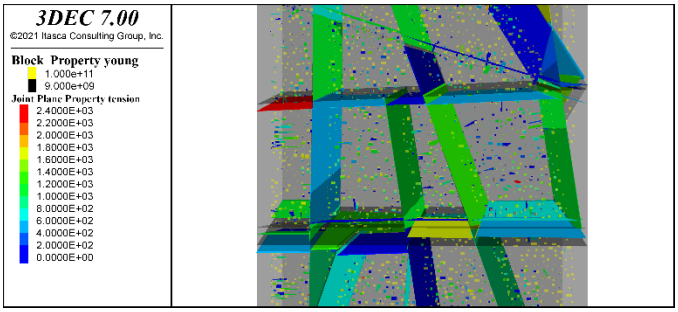

Fig. 12. Instantaneous tensile strength in mineral grain and discontinuity contacts for the case of 9% rectangular grains in a poorly cleated coal model.

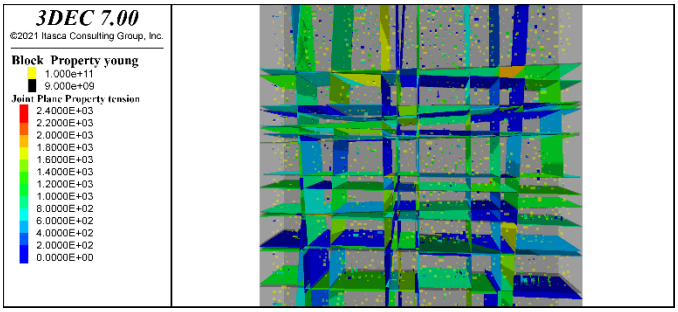

Fig. 13. Instantaneous tensile strength in mineral grains and discontinuity contacts for the case of 9% rectangular grains in a well-cleated coal model.

4. CONCLUSIONS

In this study, the effects of different shapes and distribution densities of the stiff pyrite grains in the synthetic coal were evaluated using stochastic simulations, DFNs, and 3DEC modeling techniques. This study illustrates a method with which to provide support for estimating risk of dynamic failure events from a geochemical or mineralogical perspective. We conclude that the behaviors of the synthetic coal specimens were highly correlated not only with the degree of cleats development but also with the mineral grain shape and mineral volume proportion. The results of the numerical modeling agreed well with the anisotropic characteristics, the mineral occurrence, and its impact reported in the literature. A better understanding of risk is a very critical step in improving miner safety with respect to bump potential in coal mines. However, future studies may be conducted to investigate whether this finding holds for other scales, i.e., mine-scale, as well as to assess an influence of factors not explicitly considered in this study (such as rotation angle) on synthetic coal behavior.

ACKNOWLEDGMENT

The authors greatly appreciate the help of Dr. Gabriel Walton at Colorado School of Mines who made this work possible.

DISCLAIMER

The findings and conclusions in this report are those of the author(s) and do not necessarily represent the views of the National Institute for Occupational Safety and Health. Mention of any company or product does not constitute endorsement by NIOSH.

References

Cai, Y., Liu, D., Pan, Z., Yao, Y., and Li, C. 2015. Mineral occurrence and its impact on fracture generation in selected Qinshui Basin coals: An experimental perspective. Int. J. Coal Geol., 150–151: 35–50, https://doi.org/10.1016/j.coal.2015.08.006.

Itasca Consulting Group, Inc. 2019. 3DEC distinct element modeling of jointed and blocky material in 3D. User's guide. version 7.0. Itasca Consulting Group, Inc. http://docs.itascacg.com/3dec700/3dec/docproject/source/3dechome.html.

Kim, B.-H., and Larson, M. K. 2021. Laboratory investigation of the anisotropic confinement-dependent brittle-ductile transition of a Utah coal. Int. J. Min. Sci. Technol., 31(1): 51–57, https://doi.org/10.1016/j.ijmst.2020.12.017.

Kim, B.-H., Walton, G., Larson, M. K., and Berry, S. 2018. Experimental study on the confinement-dependent characteristics of a Utah coal considering the anisotropy by cleats. Int. J. Rock Mech. Min. Sci., 105: 182–191, https://doi.org/10.1016/j.ijrmms.2018.03.018.

Kim, B. H., and Larson, M. K. 2017. Evaluation of bumps-prone potential regarding the spatial characteristics of cleat in coal pillars under highly stressed ground conditions. In Proceedings, 51st U.S. Rock Mechanics/Geomechanics Symposium. (San Francisco: June 25–28, 2017) Alexandria, VA: American Rock Mechanics Association (ARMA), 8 pp.

Lawson, H. 2020. Exploration of petrographic, elemental, and material properties of dynamic failure-prone coals. Int. J. Min. Sci. Technol., 30: 69–75.

OriginLab Corporation 2021. Origin 2021 feature highlights. OriginLab Corporation. https://www.originlab.com/2021.

Peng, S. S. 2008. Coal mine ground control. 3rd edition (Morgantown, WV: West Virginia University), 764 pp.

Ye, J., Zhang, Q., Zuo, Y., and Cheng, W. 2013. Digital-image based numerical simulation on failure process of high-sulfur coal. TELKOMNIKA Indonesian Journal of Electrical Engineering 11(1): 203–212.